

2 **Scattering of flexural wave in thin plate with multiple holes** 3 **by using the null-field integral equation approach**

4 **Wei-Ming Lee¹, Jeng-Tzong Chen²**

5 **Abstract:** In this paper, a semi-analytical approach is proposed to solve the scat-
6 tering problem of flexural waves and to determine dynamic moment concentration
7 factors (DMCFs) in an infinite thin plate with multiple circular holes. The null-field
8 integral formulation is employed in conjunction with degenerate kernels, tensor
9 transformation and Fourier series. In the proposed direct formulation, all dynamic
10 kernels of plate are expanded into degenerate forms and further the rotated degen-
11 erate kernels have been derived for the general exterior problem. By uniformly
12 collocating points on the real boundary, a linear algebraic system is constructed.
13 The results of dynamic moment concentration factors for the plate with one hole
14 are compared with the analytical solution to verify the validity of the proposed
15 method. For the cases of small wave number, the quasi-static results of a plate with
16 one or multiple circular holes are compared with the static data of finite element
17 method (FEM) using ABAQUS. Numerical results indicate that the DMCF of two
18 holes is apparently larger than that of one hole when two holes are close to each
19 other. Fictitious frequency appeared in the external problem can be suppressed by
20 using the more number of Fourier series terms. The effect of distance between the
21 centers of holes on dynamic moment concentration factors is also investigated by
22 using the proposed method.

23 **Keywords:** scattering, flexural wave, dynamic moment concentration, biHelmholtz
24 equation, null-field boundary integral equation, degenerate kernel, Fourier series

25 **1 Introduction**

26 Thin plates with multiple circular holes are widely used in engineering structures,
27 e.g. missiles, aircraft, etc., either to reduce the weight of the whole structure or
28 to increase the range of inspection. Geometric discontinuities due to these holes
29 result in the stress concentration, which reduce the load carrying capacity. The

¹ Department of Mechanical Engineering, China Institute of Technology, Taipei, Taiwan

² Department of Harbor and River Engineering, National Taiwan Ocean University, Keelung, Taiwan

30 deformation and corresponding stresses produced by the dynamic force are prop-
31 agated through the structure in the way of waves. At the irregular interface of
32 different media, stress wave reflects in all directions; this phenomenon is the scat-
33 tering. It turns out that the scattering of the stress wave results in the dynamic stress
34 concentration [Pao and Chao (1972)].

35 Nishimura *et al.* [Nishimura and Jimbo (1955)] were two of the early investigators
36 for the analytical study of the dynamic stress concentration and they determined the
37 stresses in the vicinity of a spherical inclusion in the elastic solid under a harmonic
38 force. Pao [Pao (1962)] studied the scattering of flexural waves and dynamic stress
39 concentrations around a circular hole, and proposed an analytical solution. Since
40 then, most research work has focused on the scattering of elastic wave and the re-
41 sulted dynamic stress concentration and has led to a rapid development of analyti-
42 cal or numerical approach such as the method of wave function expansion, complex
43 variable method, boundary integral equation method and boundary element method
44 [Pao and Chao (1972)].

45 Kung [Kung (1964)] studied dynamic stress concentrations resulting from the scat-
46 tering of flexural waves on the thin plate with one circular hole and gave the calcu-
47 lations of moment and shear forces as a function of frequency. Liu *et al.* [Lin, Ga
48 and Tao (1982)] extended the complex variable function approach for statics to the
49 case of dynamic loading. The dynamic stress concentration factors were given for
50 circular and elliptical cavities in an infinite plane by incident plane compressional
51 waves. By using the flux conservation relation and optical theorem, Norris *et al.*
52 [Norris and Vemula (1995)] considered the scattering of flexural waves by circular
53 inclusions with different plate properties and obtained numerical results. The com-
54 plex variable function approach and conformal mapping technique were employed
55 to solve diffraction problem of flexural waves by two cutouts [Hu, Ma and Huang
56 (1998)] and dynamic concentration factors of plates with two circular holes were
57 presented under various boundary conditions. Squire and Dixon [Squire and Dixon
58 (2000)] applied the wave function expansion method to study the scattering proper-
59 ties of a single coated cylindrical anomaly located in a thin plate on which flexural
60 waves propagate. Gao *et al.* [Gao, Wang and Ma (2001)] dealt with theoretical and
61 numerical analysis of scattering of elastic wave and dynamic stress concentrations
62 in an infinite plate with a circular hole using boundary element method. Hayir *et al.*
63 [Hayir and Bakirtas (2004)] applied the image method to analyze the scattering and
64 dynamic stress concentrations of elastic waves in plates with a circular hole subject
65 to plane harmonic SH wave. Gao *et al.* [Gao, Wang, Zhang and Ma (2005)] stud-
66 ied the scattering of flexural waves and calculated the dynamic stress concentration
67 in the thin plate with the cutout by using the dual reciprocity boundary element
68 method. Hu *et al.* [Hu, Fang and Huang (2007)] applied the image method and the

69 wave function expansion method to study the multiple scattering of flexural waves
70 in semi-infinite plates with a circular cutout. Recently, one monograph is devoted
71 to discussing the multiple scattering in acoustics, electromagnetism, seismology
72 and hydrodynamics [Martin (2006)].

73 From literature reviews stated previously, few papers except Hu *et al.* [Hu, Ma
74 and Huang (1998)] have been published to date reporting the scattering of flex-
75 ural wave in plate with more than one cutout. Furthermore, as Kobayashi *et al.*
76 [Kobayashi and Nishimura (1981)] pointed out that the integral equation method
77 seems to be most effective for two-dimensional steady-state flexural wave [Chen,
78 Fu and Zhang (2007); Chandrasekhar, Rao (2007); Chandrasekhar (2008)]. In the
79 paper, the boundary integral method is devoted to solving the multiple scattering
80 of flexural wave and dynamic stress concentrations in plate with multiple circular
81 holes.

82 It is noted that improper integrals on the boundary should be handled particularly
83 when the BEM or BIEM is used. In the past, many researchers proposed several
84 regularization techniques to deal with the singularity and hypersingularity. The de-
85 termination of the Cauchy principal value (CPV) and the Hadamard principal value
86 (HPV) in the singular and hypersingular integrals are critical issues in BEM/BIEM
87 [Chen and Hong (1999); Tanaka, Sladek and Sladek (1994)]. For the plate problem,
88 it is more difficult to calculate the principal values since the kernels are involved
89 with transcendental functions and their higher-order gradients. Readers can consult
90 with the review article by Beskos [Beskos (1997)]. In this paper, instead of using
91 the previous concepts, the kernel function is recast into the degenerate kernel which
92 is expanded into a series form on each side (interior and exterior) of the boundary
93 by employing the addition theorem since the double layer potential is discontin-
94 uous across the boundary. In reality, addition theorems are expansion formulae
95 for the special functions (e.g. Bessel function, spherical harmonics, etc.) in a se-
96 lected coordinate system [Gradshteyn and Ryzhik (1996)]. Therefore, degenerate
97 kernel, namely separable kernel, is a vital tool to study the perforated plate. Based
98 on the direct boundary integral formulation, Chen *et al.* [Chen, Shen and Chen
99 (2006a); Chen, Hsiao and Leu (2006b)] recently proposed null-field integral equa-
100 tions in conjunction with degenerate kernels and Fourier series to solve boundary
101 value problems with circular boundaries. By introducing the degenerate (separa-
102 ble) kernel, BIE involves nothing more than the linear algebra. Some applications
103 were done in the plate problems [Chen, Hsiao and Leu (2006b)] and the derivation
104 of anti-plane dynamic green's function [Chen and Ke (2008)]. The introduction of
105 degenerate kernel in companion with Fourier series was proved to yield the expo-
106 nential convergence [Kress (1989)] instead of the linear algebraic convergence in
107 BEM.

108 This paper presents a semi-analytical approach to solve scattering of flexural waves
 109 and dynamic moment concentration factors in a thin plate with multiple circu-
 110 lar holes. A linear algebraic system will be constructed by taking finite terms of
 111 Fourier series after uniformly collocating points on the boundary. After determin-
 112 ing the Fourier coefficients of unknown boundary density, the displacement and
 113 corresponding section force produced by the incident flexural wave are determined
 114 by using the boundary integral equations for the domain point. For the plate prob-
 115 lem, the slope (bending angle) and moment in the normal and tangential directions
 116 for the multiply-connected domain problem are determined with care under the
 117 adaptive observer system. Therefore, the operator of transformation matrix for the
 118 slope and moment is adopted to deal with this problem. Finally, the obtained result
 119 for an infinite plate with one circular hole is compared with the analytical solu-
 120 tion [Kung (1964)] to verify the validity of the present method. For the cases of
 121 small wave number, the results for more than one hole will be compared with those
 122 of FEM using ABAQUS to demonstrate the generality of the proposed method.
 123 Finally the effect of central distance between holes on dynamic moment concentra-
 124 tion factors is also investigated by the proposed method.

125 2 Problem statement and boundary integral formulation

126 2.1 Problem statement

The governing equation of the flexural wave for a uniform infinite thin plate with randomly distributed circular holes as shown in Figure 1 is written as follows:

$$127 \nabla^4 u(x) = k^4 u(x), \quad x \in \Omega \quad (1)$$

128 where ∇^4 is the biharmonic operator, u is the out-of-plane elastic displacement,
 129 $k^4 = \omega^2 \rho_0 h / D$, k (2π /wave length) is the wave number of elastic wave, ω is the
 130 circular frequency, ρ_0 is the volume density, $D = Eh^3 / 12(1 - \nu^2)$ is the flexural
 131 rigidity, E denotes the Young's modulus, ν is the Poisson ratio, h is the plate thick-
 132 ness and Ω is the domain of the thin plate..

132 2.2 Boundary integral equation for the collocation point in the domain

The integral representation for the plate problem can be derived from the Rayleigh-Green identity [Kitahara (1985)] as follows:

$$133 u(x) = \int_B U(s,x)v(s)dB(s) - \int_B \Theta(s,x)m(s)dB(s) + \int_B M(s,x)\theta(s)dB(s) \\ - \int_B V(s,x)u(s)dB(s), \quad x \in \Omega \quad (2)$$

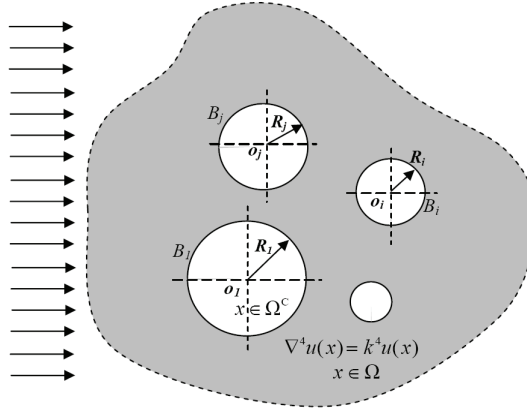


Figure 1: Problem statement for an infinite plate with multiple circular holes subject to an incident flexural wave

$$\theta(x) = \int_B U_\theta(s,x)v(s)dB(s) - \int_B \Theta_\theta(s,x)m(s)dB(s) + \int_B M_\theta(s,x)\theta(s)dB(s) - \int_B V_\theta(s,x)u(s)dB(s), \quad x \in \Omega \quad (3)$$

$$m(x) = \int_B U_m(s,x)v(s)dB(s) - \int_B \Theta_m(s,x)m(s)dB(s) + \int_B M_m(s,x)\theta(s)dB(s) - \int_B V_m(s,x)u(s)dB(s), \quad x \in \Omega \quad (4)$$

$$v(x) = \int_B U_v(s,x)v(s)dB(s) - \int_B \Theta_v(s,x)m(s)dB(s) + \int_B M_v(s,x)\theta(s)dB(s) - \int_B V_v(s,x)u(s)dB(s), \quad x \in \Omega \quad (5)$$

where B is the boundary of the domain Ω ; $u(x)$, $\theta(x)$, $m(x)$ and $v(x)$ are the displacement, slope, moment and shear force; $U(s,x)$, $\Theta(s,x)$, $M(s,x)$, $V(s,x)$, $U_\theta(s,x)$, $\Theta_\theta(s,x)$, $M_\theta(s,x)$, $V_\theta(s,x)$, $U_m(s,x)$, $\Theta_m(s,x)$, $M_m(s,x)$, $V_m(s,x)$, $U_v(s,x)$, $\Theta_v(s,x)$, $M_v(s,x)$ and $V_v(s,x)$ are kernel functions; s and x mean the source and field points, respectively. It is noted that the null field points do not include the boundary

in the conventional BIEM. But it can be done when the kernel functions in Eqs.(2)-(5) are expanded to degenerate kernels, which will be described in section 2.4. The kernel function $U(s, x)$ in Eq.(2) is the fundamental solution which satisfies

$$\nabla^4 U(s, x) - k^4 U(s, x) = \delta(s - x) \quad (6)$$

where $\delta(s - x)$ is the Dirac-delta function, respectively. Considering the two singular solutions ($Y_0(kr)$ and $K_0(kr)$, which are the zeroth-order of the second-kind Bessel and modified Bessel functions, respectively) [Hutchinson (1991)] and one regular solution ($J_0(kr)$ is the zeroth-order of the first-kind Bessel) in the fundamental solution, we have the complex-valued kernel,

$$U(s, x) = \frac{1}{8k^2 D} \left[Y_0(kr) - iJ_0(kr) + \frac{2}{\pi} K_0(kr) \right], \quad (7)$$

where $r \equiv |s - x|$ and $i^2 = -1$, which ensures the outgoing wave in companion with $e^{-i\omega t}$. The other three kernels, $\Theta(s, x)$, $M(s, x)$ and $V(s, x)$, in Eq.(2) can be obtained by applying the following slope, moment and effective shear operators defined by

$$K_{\Theta} = \frac{\partial(\cdot)}{\partial n} \quad (8)$$

$$K_M = -D \left[\nu \nabla^2(\cdot) + (1 - \nu) \frac{\partial^2(\cdot)}{\partial n^2} \right] \quad (9)$$

$$K_V = -D \left[\frac{\partial}{\partial n} \nabla^2(\cdot) + (1 - \nu) \frac{\partial}{\partial t} \left(\frac{\partial}{\partial n} \left(\frac{\partial}{\partial t}(\cdot) \right) \right) \right] \quad (10)$$

to the kernel $U(s, x)$ with respect to the source point, where $\partial/\partial n$ and $\partial/\partial t$ are the normal and tangential derivatives, respectively, ∇^2 means the Laplacian operator. In the polar coordinate of (R, θ) , the normal and tangential derivatives can be expressed by $\partial/\partial R$ and $(1/R)\partial/\partial \theta$, respectively, and then the three kernel functions can be expressed as:

$$\Theta(s, x) = K_{\Theta, s}(U(s, x)) = \frac{\partial U(s, x)}{\partial R} \quad (11)$$

$$M(s, x) = K_{M, s}(U(s, x)) = -D \left[\nu \nabla_s^2 U(s, x) + (1 - \nu) \frac{\partial^2 U(s, x)}{\partial R^2} \right] \quad (12)$$

$$\begin{aligned} V(s, x) &= K_{V, s}(U(s, x)) \\ &= -D \left[\frac{\partial}{\partial R} (\nabla_s^2 U(s, x)) + (1 - \nu) \left(\frac{1}{R} \right) \frac{\partial}{\partial \theta} \left(\frac{\partial}{\partial R} \left(\frac{1}{R} \frac{\partial U(s, x)}{\partial \theta} \right) \right) \right] \end{aligned} \quad (13)$$

The expressions for $\theta(x)$, $m(x)$ and $v(x)$ in Eqs.(3)-(5), which can be obtained by applying the operators in Eqs.(8)-(10) to $u(x)$ in Eq. (2) with respect to the field point $x(\rho, \phi)$, are

$$\theta(x) = K_{\Theta,x}(u(x)) = \frac{\partial u(x)}{\partial \rho} \quad (14)$$

$$m(x) = K_{M,x}(u(x)) = -D \left[v \nabla^2 u(x) + (1 - \nu) \frac{\partial^2 u(x)}{\partial \rho^2} \right] \quad (15)$$

$$\begin{aligned} v(x) &= K_{V,x}(u(x)) \\ &= -D \left[\frac{\partial}{\partial \rho} (\nabla_s^2 u(x)) + (1 - \nu) \left(\frac{1}{\rho} \right) \frac{\partial}{\partial \phi} \left[\frac{\partial}{\partial \rho} \left(\frac{1}{\rho} \frac{\partial u(x)}{\partial \phi} \right) \right] \right]. \quad (16) \end{aligned}$$

133 By this way, the kernel functions $U_\theta(s,x)$, $\Theta_\theta(s,x)$, $M_\theta(s,x)$, $V_\theta(s,x)$, $U_m(s,x)$,
134 $\Theta_m(s,x)$, $M_m(s,x)$, $V_m(s,x)$, $U_v(s,x)$, $\Theta_v(s,x)$, $M_v(s,x)$ and $V_v(s,x)$ can be obtained
135 by applying the operators in Eqs.(8)-(10) to $U(s,x)$, $\Theta(s,x)$, $M(s,x)$ and $V(s,x)$
136 with respect to the field point $x(\rho, \phi)$.

137 2.3 Null-field integral equations

The null-field integral equations derived by collocating the field point outside the domain (including the boundary point if exterior degenerate kernels are properly adopted) are shown as follows:

$$\begin{aligned} 0 = \int_B U(s,x)v(s)dB(s) - \int_B \Theta(s,x)m(s)dB(s) + \int_B M(s,x)\theta(s)dB(s) \\ - \int_B V(s,x)u(s)dB(s), \quad x \in \Omega^C \cup B, \quad (17) \end{aligned}$$

$$\begin{aligned} 0 = \int_B U_\theta(s,x)v(s)dB(s) - \int_B \Theta_\theta(s,x)m(s)dB(s) + \int_B M_\theta(s,x)\theta(s)dB(s) \\ - \int_B V_\theta(s,x)u(s)dB(s), \quad x \in \Omega^C \cup B, \quad (18) \end{aligned}$$

$$\begin{aligned} 0 = \int_B U_m(s,x)v(s)dB(s) - \int_B \Theta_m(s,x)m(s)dB(s) + \int_B M_m(s,x)\theta(s)dB(s) \\ - \int_B V_m(s,x)u(s)dB(s), \quad x \in \Omega^C \cup B, \quad (19) \end{aligned}$$

$$0 = \int_B U_v(s,x)v(s)dB(s) - \int_B \Theta_v(s,x)m(s)dB(s) + \int_B M_v(s,x)\theta(s)dB(s) - \int_B V_v(s,x)u(s)dB(s), \quad x \in \Omega^C \cup B, \quad (20)$$

138 where Ω^C is the complementary domain of Ω . Once kernel functions are expressed
 139 in proper degenerate forms, which will be described in the next subsection, the
 140 collocation points can be exactly located on the real boundary, that is $x \in \Omega^C \cup B$.
 141 Since the four equations of Eqs.(17)-(20) in the plate formulation are provided,
 142 there are 6 (C_2^4) options for choosing any two equations to solve the problems.

143 **2.4 Degenerate kernels and Fourier series for boundary densities**

In the plane polar coordinate, the field point and source point can be expressed as
 (ρ, ϕ) and (R, θ), respectively. By applying the addition theorem [Gradshteyn and
 Ryzhik (1996)] to Eq. (7), the degenerated form for the kernel function $U(s,x)$ can
 be expressed in the series form as follows

$$U : \begin{cases} U^I(s,x) = \frac{1}{8k^2D} \sum_{m=0}^{\infty} \varepsilon_m \{J_m(k\rho)[Y_m(kR) - iJ_m(kR)] \\ \quad + \frac{2}{\pi} I_m(k\rho)K_m(kR)\} \cos [m(\theta - \phi)], \quad \rho < R \\ U^E(s,x) = \frac{1}{8k^2D} \sum_{m=0}^{\infty} \varepsilon_m \{J_m(kR)[Y_m(k\rho) - iJ_m(k\rho)] \\ \quad + \frac{2}{\pi} I_m(kR)K_m(k\rho)\} \cos [m(\theta - \phi)], \quad \rho \geq R \end{cases} \quad (21)$$

144 where ε_m is the Neumann factor ($\varepsilon_m=1, m=0; \varepsilon_m=2, m=1,2,\dots, \infty$) and the super-
 145 scripts “I” and “E” denote the interior and exterior cases for $U(s,x)$ degenerate
 146 kernels to distinguish $\rho < R$ and $\rho > R$, respectively as shown in Figure 2. The
 147 degenerate kernels $\Theta(s,x)$, $M(s,x)$ and $V(s,x)$ in the null-field boundary integral
 148 equations can be obtained by applying the operators of Eqs.(8)-(10) to the degen-
 149 erate kernel $U(s,x)$, given by Eq.(21), with respect to the source point s . The
 150 other degenerate kernels $U_\theta(s,x)$, $\Theta_\theta(s,x)$, $M_\theta(s,x)$, $V_\theta(s,x)$, $U_m(s,x)$, $\Theta_m(s,x)$,
 151 $M_m(s,x)$, $V_m(s,x)$, $U_v(s,x)$, $\Theta_v(s,x)$, $M_v(s,x)$ and $V_v(s,x)$ can be obtained by apply-
 152 ing the operators of Eqs.(8)-(10) to the degenerate kernel $U(s,x)$, $\Theta(s,x)$, $M(s,x)$
 153 and $V(s,x)$ with respect to the field point x . The expressions of these degenerate
 154 kernels are listed in the Appendix \mathcal{A}^1 .

In order to fully utilize the geometry of circular boundary, the displacement $u(s)$,
 slope $\theta(s)$, moment $m(s)$ and shear force $v(s)$ along the circular boundaries in
 the null-field integral equations are represented by using Fourier series expansion,

respectively, as shown below:

$$u(s) = u_{c0} + \sum_{n=1}^M (u_{cn} \cos n\theta + u_{sn} \sin n\theta), \quad s \in B, \quad (22)$$

$$\theta(s) = \theta_{c0} + \sum_{n=1}^M (\theta_{cn} \cos n\theta + \theta_{sn} \sin n\theta), \quad s \in B, \quad (23)$$

$$m(s) = m_{c0} + \sum_{n=1}^M (m_{cn} \cos n\theta + m_{sn} \sin n\theta), \quad s \in B, \quad (24)$$

$$v(s) = v_{c0} + \sum_{n=1}^M (v_{cn} \cos n\theta + v_{sn} \sin n\theta), \quad s \in B, \quad (25)$$

155 where u_{c0} , u_{cn} , u_{sn} , θ_{c0} , θ_{cn} , θ_{sn} , m_{c0} , m_{cn} , m_{sn} , v_{c0} , v_{cn} and v_{sn} are the Fourier
 156 coefficients and M is the truncated number of Fourier series terms. The number of
 157 terms M in the Fourier series for circular boundaries can be, in general, different for
 158 each boundary circle. For simplicity, we used the same number of Fourier terms for
 159 each circular boundary. By using degenerated kernels, Fourier series and orthogo-
 160 nal property, all the improper integrals in Eqs.(17)-(20) can be transformed to series
 161 sum and then be calculated easily, since the potential across the boundary can be
 162 described by using the degenerate kernel with series form in each side. Successful
 163 experiences on Laplace problems [Chen, Shen and Chen (2006a)], Helmholtz prob-
 164 lems [Chen \times 4 (2007)] and biharmonic problems [Chen, Hsiao and Leu (2006b)]
 165 can be found.

166 3 Adaptive observer system and transformation of tensor components

167 3.1 Adaptive observer system

168 For the direct boundary integral equations being frame indifferent (*i.e.* rule of ob-
 169 jectivity), the origin of the observer system can be adaptively located on the center
 170 of the corresponding boundary contour under integration. Adaptive observer sys-
 171 tem is chosen to fully employ the circular property, which takes the full advantage
 172 of both Fourier series to represent boundary variables and degenerate-kernel ex-
 173 pressions in the polar coordinate. Figure 3 shows the boundary integration for the
 174 circular boundaries in the adaptive observer system. The dummy variable in the
 175 circular contour integration is only the angle θ . By using the adaptive system, all
 176 the boundary integrals can be determined analytically free of calculating principal
 177 value.

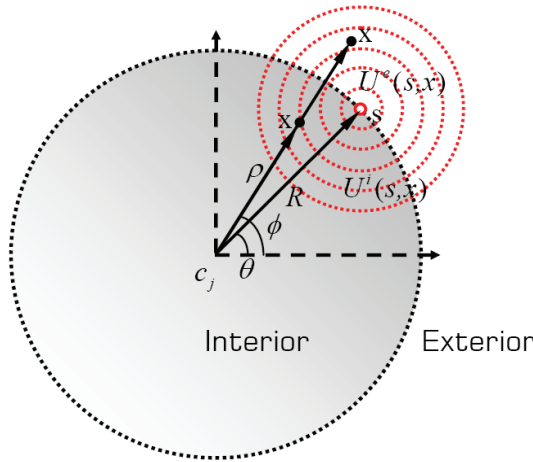


Figure 2: Degenerate kernel for $U(s, x)$

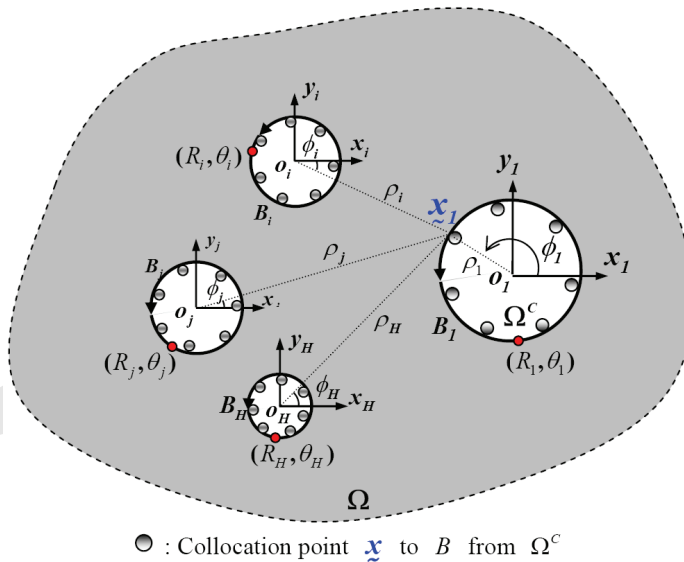


Figure 3: Collocation point and boundary contour integration in the boundary integral equation by using the adaptive observer system

178 **3.2 Transformation of tensor components**

For the slope, moment and effective shear force being calculated in the plate problem, special treatment for the potential gradient or higher-order gradient should be

taken care as the source and field points locate on different circular boundaries. As shown in Figure 4, the angle ϕ_i is polar coordinate of the collocation point x_i centered at o_i which locate the center of the circle under integration and the angle ϕ_c is that centered at o_j being the center of the circle on which collocation point is located. According to the transformation law for the components of tensor, we have

$$\begin{bmatrix} (\cdot)_n \\ (\cdot)_t \end{bmatrix} = \begin{bmatrix} \cos(\delta) & \sin(\delta) \\ -\sin(\delta) & \cos(\delta) \end{bmatrix} \begin{bmatrix} (\cdot)_r \\ (\cdot)_\theta \end{bmatrix} \quad (26)$$

$$\begin{bmatrix} (\cdot)_{nn} \\ (\cdot)_{tt} \\ (\cdot)_{nt} \end{bmatrix} = \begin{bmatrix} \cos^2(\delta) & \sin^2(\delta) & 2\sin(\delta)\cos(\delta) \\ \sin^2(\delta) & \sin^2(\delta) & -2\sin(\delta)\cos(\delta) \\ -\sin(\delta)\cos(\delta) & \sin(\delta)\cos(\delta) & \cos^2(\delta) - \sin^2(\delta) \end{bmatrix} \begin{bmatrix} (\cdot)_{rr} \\ (\cdot)_{\theta\theta} \\ (\cdot)_{r\theta} \end{bmatrix}. \quad (27)$$

Based on Eqs. (26) and (27), the general rotated slope, normal bending and tangential bending moment kernels can be obtained by following operators:

$$K_{\Theta}^R = \cos(\delta) \frac{\partial(\cdot)}{\partial n} + \sin(\delta) \frac{\partial(\cdot)}{\partial t} \quad (28)$$

$$K_N^R = -D \left\{ [v + (1 - v) \sin^2(\delta)] \nabla^2(\cdot) + \cos(2\delta)(1 - v) \frac{\partial^2(\cdot)}{\partial n^2} + \sin(2\delta)(1 - v) \frac{\partial}{\partial n} \left(\frac{\partial(\cdot)}{\partial t} \right) \right\} \quad (29)$$

$$K_T^R = -D \left\{ [v + (1 - v) \cos^2(\delta)] \nabla^2(\cdot) + \cos(2\delta)(v - 1) \frac{\partial^2(\cdot)}{\partial n^2} - \sin(2\delta)(1 - v) \frac{\partial}{\partial n} \left(\frac{\partial(\cdot)}{\partial t} \right) \right\} \quad (30)$$

179 where $\delta = \phi_c - \phi_i$. When the angle ϕ_c equals to the angle ϕ_i or two circles co-
 180 incide, the angle difference δ equals to zero and Eqs.(28) and (29) are simplified
 181 to Eqs.(8) and (9), respectively. The expressions of rotated degenerate kernels,
 182 $U_\theta(s, x)$, $\Theta_\theta(s, x)$, $M_\theta(s, x)$, $V_\theta(s, x)$, $U_m(s, x)$, $\Theta_m(s, x)$, $M_m(s, x)$, $V_m(s, x)$, $U_t(s, x)$,
 183 $\Theta_t(s, x)$, $M_t(s, x)$ and $V_t(s, x)$, can be obtained by applying the operators of Eqs.(28),
 184 (29) and (30) to the degenerate kernel $U(s, x)$, $\Theta(s, x)$, $M(s, x)$ and $V(s, x)$ with re-
 185 spect to the field point x and are listed in the Appendix \mathcal{A}^o .

186 4 Linear algebraic systems

Consider an infinite plate containing H nonoverlapping circular holes centered at the position vector o_j ($j=1, 2, \dots, H$), as shown in Fig. 3 in which R_j denotes

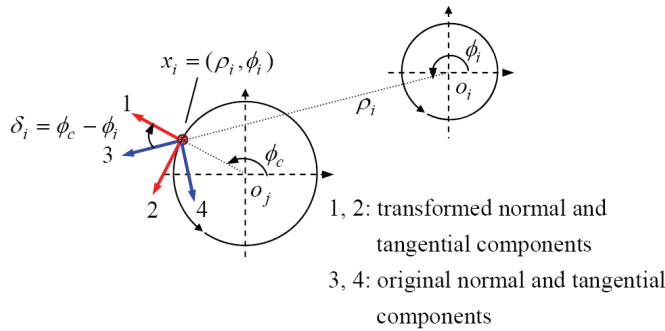


Figure 4: Transformation of tensor components

the radius of the j th circular region, x_j is the collocation point on the j th circular boundary and B_j is the boundary of the j th circular hole. Kernels of Eqs. (19) and (20) involve higher-order derivatives, which may decrease both the convergence rate and computational efficiency. For the purpose of computational efficiency, Eqs. (17) and (18) are used to analyze the plate problem. By uniformly collocating $N (=2M+1)$ points on each circular boundary in Eqs. (17) and (18), we have

$$0 = \sum_{j=1}^H \int_{B_j} \{U(s,x)v(s) - \Theta(s,x)m(s) + M(s,x)\theta(s) - V(s,x)u(s)\} dB_j(s),$$

$$x \in \Omega^C, \quad (31)$$

$$0 = \sum_{j=1}^H \int_{B_j} \{U_\theta(s,x)v(s) - \Theta_\theta(s,x)m(s) + M_\theta(s,x)\theta(s) - V_\theta(s,x)u(s)\} dB_j(s),$$

$$x \in \Omega^C. \quad (32)$$

For the B_j circular boundary integrals, the degenerate kernels of $U(s,x)$, $\Theta(s,x)$, $M(s,x)$, $V(s,x)$, $U_\theta(s,x)$, $\Theta_\theta(s,x)$, $M_\theta(s,x)$ and $V_\theta(s,x)$ are utilized and boundary densities $u(s)$, $\theta(s)$, $m(s)$ and $v(s)$ along the circular boundary are represented by using the Fourier series of Eqs.(22)-(25), respectively. By using the conventional boundary integral equations to solve a problem, the determination of the Cauchy principal value (CPV) and the Hadamard principal value (HPV) for boundary integrals of various kernel functions are inevitable. By using the addition theorem, the kernel functions in our method are expanded in the series form and the boundary integrals can be easily calculated using the series sum free of facing principal values. The selection of interior or exterior degenerate kernel depends on $\rho < R$

or $\rho > R$, respectively, according to the observer system. In the B_j integration, the origin of the observer system is adaptively set to collocate at the center o_j from which the degenerate kernels and Fourier series are described. By using orthogonal property, a linear algebraic system can be written as follows:

$$\begin{aligned}
 & \begin{bmatrix} U^{11} & -\Theta^{11} & U^{12} & -\Theta^{12} & \dots & U^{1H} & -\Theta^{1H} \\ U_{\theta}^{11} & -\Theta_{\theta}^{11} & U_{\theta}^{12} & -\Theta_{\theta}^{12} & \dots & U_{\theta}^{1H} & -\Theta_{\theta}^{1H} \\ U^{21} & -\Theta^{21} & U^{22} & -\Theta^{22} & \dots & U^{2H} & -\Theta^{2H} \\ U_{\theta}^{21} & -\Theta_{\theta}^{21} & U_{\theta}^{22} & -\Theta_{\theta}^{22} & \dots & U_{\theta}^{2H} & -\Theta_{\theta}^{2H} \\ \vdots & \vdots & \vdots & \vdots & \ddots & \vdots & \vdots \\ U^{H1} & -\Theta^{H1} & U_{\theta}^{H2} & -\Theta_{\theta}^{H2} & \dots & U^{HH} & -\Theta^{HH} \\ U_{\theta}^{H1} & -\Theta_{\theta}^{H1} & U_{\theta}^{H2} & -\Theta_{\theta}^{H2} & \dots & U_{\theta}^{HH} & -\Theta_{\theta}^{HH} \end{bmatrix} \begin{Bmatrix} v^1 \\ m^1 \\ v^2 \\ m^2 \\ \vdots \\ v^H \\ m^H \end{Bmatrix} \\
 & = \begin{bmatrix} -M^{11} & V^{11} & -M^{12} & V^{12} & \dots & -M^{1H} & V^{1H} \\ -M_{\theta}^{11} & V_{\theta}^{11} & -M_{\theta}^{12} & V_{\theta}^{12} & \dots & -M_{\theta}^{1H} & V_{\theta}^{1H} \\ -M^{21} & V^{21} & -M^{22} & V^{22} & \dots & -M^{2H} & V^{2H} \\ -M_{\theta}^{21} & V_{\theta}^{21} & -M_{\theta}^{22} & V_{\theta}^{22} & \dots & -M_{\theta}^{2H} & V_{\theta}^{2H} \\ \vdots & \vdots & \vdots & \vdots & \ddots & \vdots & \vdots \\ -M^{H1} & V^{H1} & -M_{\theta}^{H2} & V_{\theta}^{H2} & \dots & -M^{HH} & V^{HH} \\ -M_{\theta}^{H1} & V_{\theta}^{H1} & -M_{\theta}^{H2} & V_{\theta}^{H2} & \dots & -M_{\theta}^{HH} & V_{\theta}^{HH} \end{bmatrix} \begin{Bmatrix} \theta^1 \\ u^1 \\ \theta^2 \\ u^2 \\ \vdots \\ \theta^H \\ u^H \end{Bmatrix} \quad (33)
 \end{aligned}$$

where H denotes the number of circular boundaries. For brevity, a unified form $[U^{ij}]$ ($i = 1, 2, 3, \dots, H$ and $j = 1, 2, 3, \dots, H$) denote the response of $U(s, x)$ kernel at the i th circle point due to the source at the j th circle. Otherwise, the same definition is for $[\Theta^{ij}]$, $[M^{ij}]$, $[V^{ij}]$, $[U_{\theta}^{ij}]$, $[\Theta_{\theta}^{ij}]$, $[M_{\theta}^{ij}]$ and $[V_{\theta}^{ij}]$ kernels. The explicit expressions for sub-vectors $[u^i]$, $[\theta^i]$, $[m^i]$ and $[v^i]$ can be described as follows:

$$u^i = \begin{Bmatrix} u_{c0}^i \\ u_{c1}^i \\ u_{s1}^i \\ \vdots \\ u_{cM}^i \\ u_{sM}^i \end{Bmatrix}, \quad \theta^i = \begin{Bmatrix} \theta_{c0}^i \\ \theta_{c1}^i \\ \theta_{s1}^i \\ \vdots \\ \theta_{cM}^i \\ \theta_{sM}^i \end{Bmatrix}, \quad m^i = \begin{Bmatrix} m_{c0}^i \\ m_{c1}^i \\ m_{s1}^i \\ \vdots \\ m_{cM}^i \\ m_{sM}^i \end{Bmatrix}, \quad v^i = \begin{Bmatrix} v_{c0}^i \\ v_{c1}^i \\ v_{s1}^i \\ \vdots \\ v_{cM}^i \\ v_{sM}^i \end{Bmatrix}. \quad (34)$$

The explicit expressions for the sub-matrices of $[U^{ij}]$, $[\Theta^{ij}]$, $[M^{ij}]$, $[V^{ij}]$, $[U_{\theta}^{ij}]$,

$[\Theta_\theta^{ij}]$, $[M_\theta^{ij}]$ and $[V_\theta^{ij}]$ can be written as shown below

$$K^{ij} = \begin{bmatrix} K_{0C}^{ij}(\rho_1, \phi_1) & K_{1C}^{ij}(\rho_1, \phi_1) & K_{1S}^{ij}(\rho_1, \phi_1) & \cdots & K_{MS}^{ij}(\rho_1, \phi_1) \\ K_{0C}^{ij}(\rho_2, \phi_2) & K_{1C}^{ij}(\rho_2, \phi_2) & K_{1S}^{ij}(\rho_2, \phi_2) & \cdots & K_{MS}^{ij}(\rho_2, \phi_2) \\ \vdots & \vdots & \vdots & \vdots & \vdots \\ \vdots & \vdots & \vdots & \vdots & \vdots \\ K_{0C}^{ij}(\rho_N, \phi_N) & K_{1C}^{ij}(\rho_N, \phi_N) & K_{1S}^{ij}(\rho_N, \phi_N) & \cdots & K_{MS}^{ij}(\rho_N, \phi_N) \end{bmatrix}_{N \times N} \quad (35)$$

where K can be either one of $U(s, x)$, $\Theta(s, x)$, $M(s, x)$, $V(s, x)$, $U_\theta(s, x)$, $\Theta_\theta(s, x)$, $M_\theta(s, x)$ and $V_\theta(s, x)$. The notations ϕ_k and ρ_k ($k = 1, 2, 3, \dots, N$) shown in Fig. 3 are the angle and radius of the k -th collocation point on the i -th circular boundary with respect to the center of the j -th circular boundary (the origin of the observer system) and the element of the sub-matrices can be determined by

$$K_{nC}^{ij}(\rho_k, \varphi_k) = \int_0^{2\pi} K(R_j, \theta_j; \rho_k, \varphi_k) \cos(n\theta_j) (R_j d\theta_j), \quad n = 0, 1, 2, \dots, M, \quad (36)$$

$$K_{nS}^{ij}(\rho_k, \varphi_k) = \int_0^{2\pi} K(R_j, \theta_j; \rho_k, \varphi_k) \sin(n\theta_j) (R_j d\theta_j), \quad n = 1, 2, \dots, M \quad (37)$$

187 in which the selection of interior or exterior degenerate kernel depends on the po-
 188 sition of collocation point with respective to the center of circle under integration
 189 as shown in Fig. 3.

190 **5 Dynamic moment concentration factor and techniques for solving scatter-**
 191 **ing problems**

192 Considering an infinite thin plate with multiple holes subject to incident flexural
 193 wave, the boundary conditions of the hole are free. For this scattering problem, it
 194 can be decomposed into two parts, (a) incident wave field and (b) radiation field,
 195 as shown in Fig. 5. For matching the boundary conditions, the radiation boundary
 196 condition in part (b) is obtained as the minus quantity of incident wave function,
 197 e.g. $m^R = -m^I$; $v^R = -v^I$ for the free edge where the superscripts R and I denote
 198 radiation and incidence, respectively. By substituting the known radiation boundary
 199 conditions, $-m^I$ and $-v^I$, into the left hand side of Eq. (33), the unknown boundary
 200 data, u and θ , can be solved. After calculating the displacement, slope, moment
 201 and effective shear force along the boundary, the radiation field can be solved by
 202 employing the boundary integral equation for the domain point of Eqs. (2)-(5). The
 203 scattering field is determined by superimposing radiation field and incident field.
 204 The tangential bending moment $M_t(x)$ can be determined by applying the operator
 205 in Eq.(30) to Eq.(2) with respective to the field point.

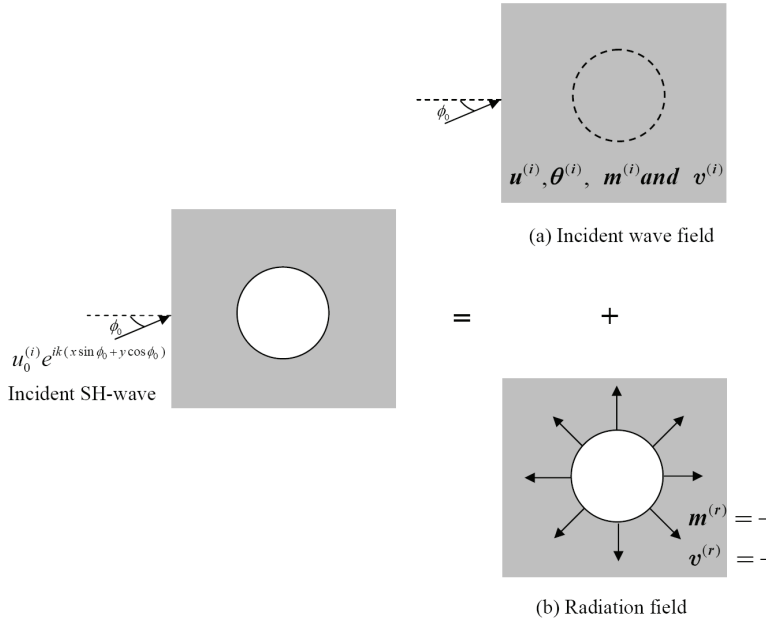


Figure 5: The decompositon of scattering problem into (a) incident wave field and (b) radition field

An incident flexural wave is represented by

$$u_0^{(i)} e^{ik(x\cos(\phi_0)+y\sin(\phi_0))} \quad (38)$$

where $u_0^{(i)}$ is the amplitude of incident wave, k is the wave number and ϕ_0 is the incident angle. Under the polar coordinate, the bending moment and effective shear force induced by the incident wave can be determined by substituting Eq. (38) into Eqs.(15) and (16). By setting the amplitude of incident wave $u_0^{(i)} = 1$, the amplitude of moment produced by the incident wave is

$$M_0 = Dk^2 \quad (39)$$

The dynamic moment concentration factor (DMCF) at any field point x can be determined as

$$DMCF(x) = M_t(x)/M_0 \quad (40)$$

206 6 Numerical results and discussions

207 Scattering problems of flexural wave in thin plate with multiple holes are solved
 208 and dynamic moment concentration factors (DMCFs) around the circular holes are

209 determined by using the present method. For the cases of small wave number, the
 210 same plate problem is independently solved by using FEM (the ABAQUS software)
 211 for comparison. In all cases, the inner boundary is subject to the free boundary
 212 condition and the thickness of plate is 0.002m. The triangular general-purpose
 213 shell element, S3, of ABAQUS was used to model the plate problem. Although the
 214 thickness of the plate is 0.002 m, these elements do not suffer from transverse shear
 215 locking according to the theoretical manual of ABAQUS.

216 *Case 1: An infinite plate with one hole* [Pao and Mow (1972); Kung (1964); Norris
 217 and Vemula (1995); Gao, Wang and Ma (2001); Gao, Wang, Zhang and Ma (2005)]

218 An infinite plate with one hole (radius $a = 1m$) subject to the incident flexural
 219 wave with $\phi_0 = 0$ is considered as shown in Figure 6. Since the analytical solution
 220 of this problem is available, convergence analysis is firstly conducted. Figure 7
 221 shows the DMCF on the circular boundary, at $\pi/2$, versus the dimensionless wave
 222 number by using different number of terms of Fourier series. From the convergence
 223 analysis, the required number of terms to approach the analytical solution increase
 224 as the incident wave number becomes larger. Results of the present method match
 225 well with those of analytical solution when the number of terms of Fourier series
 226 amounts to $M = 10$. The convergence analysis indicates that results using Fourier
 227 series with $M = 2$ match well with the analytical solution when the wave number is
 228 0.005. For the case of the higher wave number $k = 3.0$, more number of terms are
 229 required to the same extent of convergence, which shows the consistency with the
 230 results presented by Figure 7.

231 In the limit of zero wave number [Pao and Mow (1972); Kung (1964)] like k
 232 $= 0.005$, the excitation of incident wave is equivalent to the loading with static
 233 moment $M_{xx} = M_0$ and $M_{yy} = \nu M_0$ at the four sides of a plate. Accordingly, a
 234 $16m \times 16m$ plate with one hole subject to static bending moments, $M_{xx} = 1.0$ and
 235 $M_{yy} = 0.3$ at the four sides was considered. For this equivalent static case, 25567
 236 triangle elements were used to generate the FEM model and Figure 8(a) shows the
 237 corresponding result of the normalized tangential bending moment around the hole.
 238 By using the present method, the unknown boundary densities of the plate are ex-
 239 pressed in terms of Fourier series and the numerical result of DMCF around the
 240 hole using Fourier series terms ($M = 10$) is shown in Figure 8(b). The analytical
 241 solution [Pao and Mow (1972); Kung (1964)] is also shown in Figure 8(c) and good
 242 agreements are made after comparing with three different approaches stated above.

243 Figure 9 shows that the real and imaginary parts of DMCF on the circular bound-
 244 ary at $\pi/2$ versus the dimensionless wave number for various Poisson ratios by
 245 using the present method and the analytical solution [Pao and Mow (1972); Kung
 246 (1964)]. It indicates that both results match well and DMCF depends on the Pois-
 247 son ratio of the plate as well as the incident wave number. For dimensionless wave

248 number $ka=3.0$, the real and imaginary parts of DMCF along the circular boundary
 249 is shown in Figures 10, which agrees with the result reported in Gao *et al.* [Gao,
 250 Wang, Zhang and Ma (2005)]. The value of DMCF is symmetrical to x-axis due
 251 to the incident wave with $\phi_0 = 0$. Table 1 lists dynamic moment concentration fac-
 252 tors on the circular boundary ($\theta = \pi/2$) by using four approaches, dual reciprocity
 253 boundary element method [Gao, Wang, Zhang and Ma (2005)], boundary element
 254 method based on dynamic fundamental solution [Gao, Wang and Ma (2001)], the
 255 present method and the analytical solution [Pao and Mow (1972); Kung (1964)],
 256 respectively. In addition to the required number of Fourier series terms to conver-
 257 gence, results of the present method are the same as the analytical solutions up to
 258 four digits. The present method is obviously superior to the BEM thanks to the
 259 semi-analytical procedure.

For the most part of scattering applications, it is interesting to measure the scattered
 field far away from the scatter. On the other hand, the asymptotic behavior or
 uniqueness of fundamental solutions or kernel functions is an important issue for
 the numerical computation. Therefore, we examine the behavior of the scattered
 response in the far field. The scattered far field amplitude $f(\theta)$ [Norris and Vemula
 (1995)] in our approach is defined as

$$f(\theta) = \lim_{\rho \rightarrow \infty} \sqrt{2\rho} \cdot u^{(r)}(\rho) \quad (41)$$

260 where $u^{(r)}$ is the out-of-plane elastic displacement of radiation field and ρ is the
 261 radius of the field point. In the computation, the radius of the field point is taken
 262 90m because $f(\theta)$ converges a steady value when this radius is more than about
 263 90m. Figure 11 shows a polar plot of the far field scattering amplitude for a circular
 264 hole in a 0.025m steel plate, solid line for $ka = 1.0$, dash line for $ka = 0.5$. Figure
 265 12 presents the far field backscattered amplitude versus the dimensionless wave
 266 number for an incident wave of unit amplitude, solid line for the hole, dash line
 267 for the rigid inclusion. The rigid inclusion means the clamped boundary condition
 268 around the circular boundary. As the dimensionless wave number becomes large,
 269 results of both cases approach the same value of one. The results for the hole
 270 show a local maximum near the small wave number and then increase with the
 271 wave number, which consists with the results shown in Figure 11. The results
 272 match well with those of Norris and Vemula [Norris and Vemula (1995)]. It can be
 273 found that the amplitude for the radiation (or scattering) response in the far field is
 274 $O(\rho^{-1/2})$, which satisfy the radiation condition.

275 *Case 2: An infinite plate with two holes* [Hu, Ma and Huang (1998)]

276 An infinite plate with two holes (radius $a = 1m$) subject to the incident flexural wave
 277 with $\phi_0 = 0$ is considered as shown in Figure 13, where L is the central distance

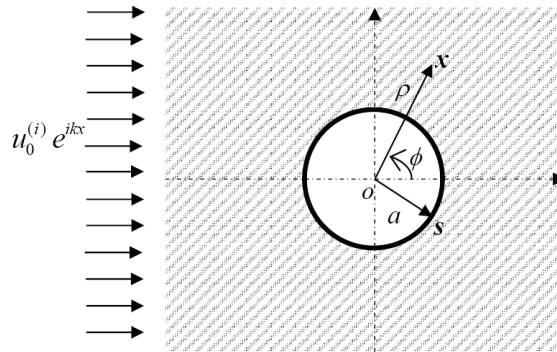


Figure 6: An infinite plate with one hole subject to an incident flexural wave

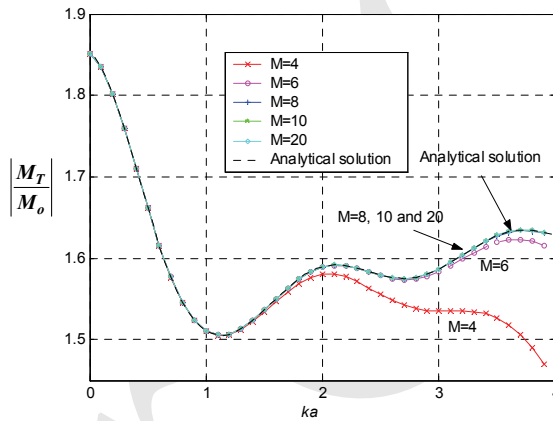


Figure 7: Dynamic moment concentration factor on the circular boundary ($\theta = \pi/2$) versus the dimensionless wave number by using different number of terms of Fourier series

278 of two holes. For the case of $L = 2.1m$, Figure 14 shows the DMCF on the upper
 279 circular boundary, at $-\pi/2$, versus the dimensionless wave number by using dif-
 280 ferent number of Fourier series terms. From this convergence analysis, the results
 281 using fewer Fourier series terms show some peaks at $ka=3.2, 4.6$. Even so, the con-
 282 vergence is fast achieved when the number of Fourier series terms M amounts to
 283 twenty. Values of wave number corresponding to those peaks are found to be equal
 284 to the true eigenvalues of the clamped circular plate with a radius equaling to that of
 285 the hole, i.e. 3.196, 4.610 [Leissa (1969)]. Actually they are the so-called fictitious
 286 frequencies of the external problem. It demonstrates that the increasing number of

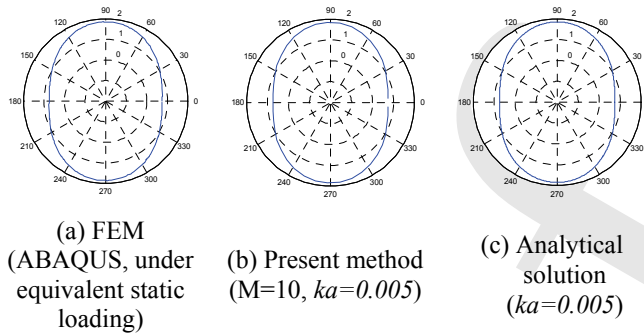


Figure 8: Distribution of dynamic moment concentration factors on the circular boundary by using different methods, the present method, analytical solution and FEM

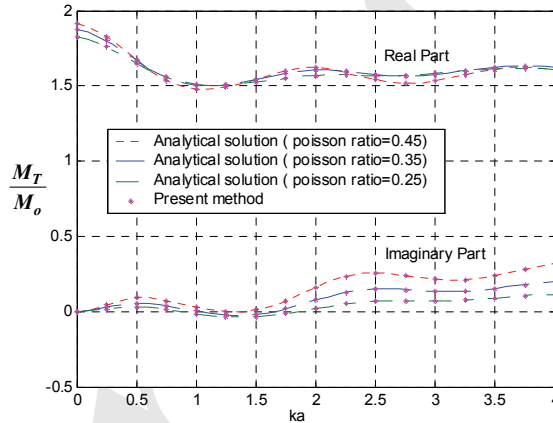


Figure 9: The real and imaginary parts of DMCF on the circular boundary ($\theta = \pi/2$) versus the dimensionless wave number for different Poisson ratios

287 Fourier series terms can suppress the appearance of fictitious frequencies.

288 For comparison with the proposed method, we consider a $16m \times 22m$ plate with
 289 two holes ($L = 2.1m$) subject to static bending moments, $M_{xx} = 1.0$ and $M_{yy} = 0.3$
 290 at the four sides. For this case, 49024 triangle elements were used to generate
 291 the FEM model and the corresponding result of the normalized tangential bending
 292 moment around the hole is shown in Figure 15(a). The result of the present method
 293 for $k = 0.005$ is also shown in Figure 15(b) and good agreements are made after
 294 comparison. It indicates that the maximum DMCF is larger than that of one hole
 295 shown in Figure (8) due to two close holes in this case.

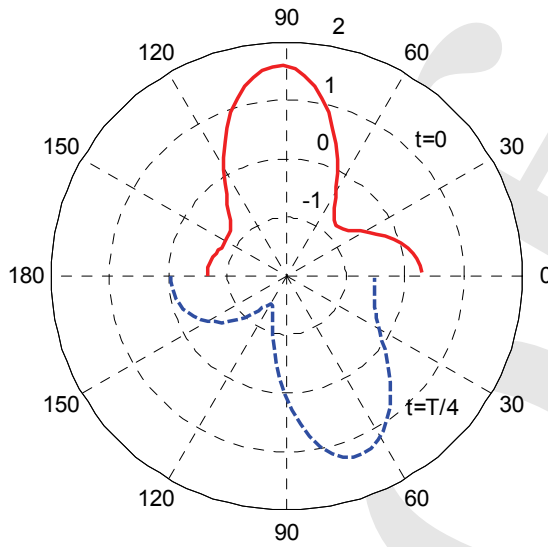


Figure 10: Distribution of DMCF (M_T/M_0) on the circular boundary, solid line (real part) for $t = 0$ for, dash line (imaginary part) for $t = T/4$ ($ka = 3.0$)

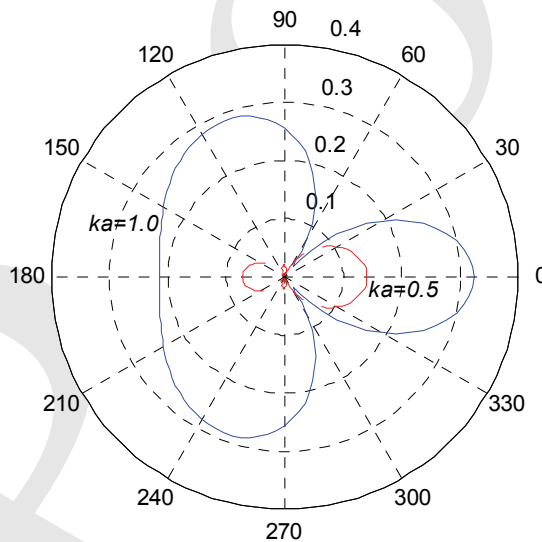


Figure 11: A polar plot of the far field scattering amplitude for a circular hole in a 0.025m steel plate, solid line for $ka = 1.0$, dash line for $ka = 0.5$

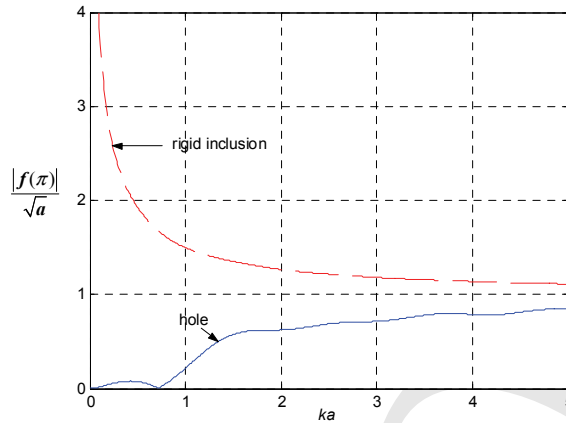


Figure 12: The magnitude of the backscattered far field flexural response for an incident wave of unit amplitude. The surrounding plate is steel of thickness 0.025m, solid line for hole, dash line for rigid inclusion

Table 1: Dynamic moment concentration factor on the circular boundary ($\theta = \pi/2$)

k	$f = 1 + r^*$	$f = 1 - r - r^*$	Ref **	Present method	Analytical solution
0.1	1.8285	1.8301	1.8360	1.8353(4)	1.8353(4)
0.5	1.6681	1.6692	1.6710	1.6616(6)	1.6616(6)
1.0	1.6452	1.6437	1.6420	1.5109(6)	1.5109(6)
2.0	1.6439	1.6458	1.6550	1.5894(8)	1.5894(8)
3.0	1.6475	1.6483	1.6500	1.5868(12)	1.5868(12)
5.0	1.6503	1.6509	1.6520	1.6305(14)	1.6305(14)

() denotes the required number of terms to converge the steady result within four digits.

* refer to the results [Gao, Wang, Zhang and Ma (2005)]

** refer to the results [Gao, Wang and Ma (2001)]

296 For the case of $L = 4.0m$, Figure 16 shows the DMCF on the upper circular bound-
 297 ary, at $-\pi/2$, versus the dimensionless wave number by using different number of
 298 terms of Fourier series. Instead of peak appeared in Figure 14, the result of con-
 299 vergence is similar to that of the case with one hole shown in Figure 7 due to two
 300 holes separated apparently.

301 For dimensionless incident wave number $ka=0.2$ with the central distance between
 302 two holes $L=2.1a$, Figure 17 shows the distribution of the amplitude of DMCF on

303 the circular boundary, solid line for one hole and dash line for the upper one of two
 304 holes. The DMCF of two holes is apparently larger than that of one hole when two
 305 holes are close each other.

306 Figure 18 shows the DMCF at the upper circular edge ($-\pi/2$) versus the dimensionless
 307 central distance under different incident wave number, where the dot line
 308 denotes the corresponding results for one hole case. It indicates that when the central
 309 distance between two holes gradually increases, the results for the case of two
 310 holes approach that of the case with one hole. For the case of $k=2.0$, oscillation
 311 behavior of DMCF is observed as the central distance of two holes varies. It is
 312 not found for the cases with the small wave number such as $ka=0.1, 0.2$ and 0.5 .
 313 Furthermore, we zoom in the data of $ka=0.1$ at upper right corner (in the range of
 314 1.834 to 1.838 for $|M_T/M_0|$). Then, it is refound that the oscillation behavior of
 315 DMCF with a period $2\pi/k$ versus L/a for all wave numbers appears, which was
 not found in Hu *et al.* [Hu, Ma and Huang (1998)]

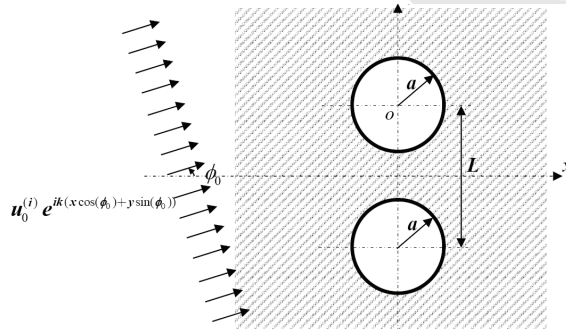


Figure 13: An infinite plate with two holes subject to an incident flexural wave with an incident angle ϕ_0

316

317 7 Conclusions

318 A semi-analytical approach to solve the scattering problem of flexural waves and
 319 to determine dynamic moment concentration factors in an infinite thin plate with
 320 multiple circular holes was proposed. The radiation field was determined by em-
 321 ploying the null-field integral formulation in conjunction with degenerate kernels,
 322 tensor transformation and Fourier series. All the improper integrals in the null-
 323 field integral formulation were avoided by using the degenerate kernels and were
 324 easily calculated through the series sum. For the general exterior case, the rotated
 325 degenerate kernels have been derived in the adaptive observer system. Once the

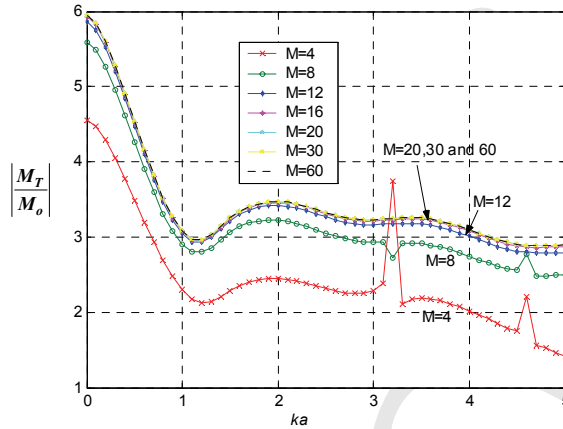


Figure 14: DMCF on the upper circular boundary ($\theta = -\pi/2$) versus the dimensionless wave number by using different number of terms of Fourier series ($L/a=2.1$)

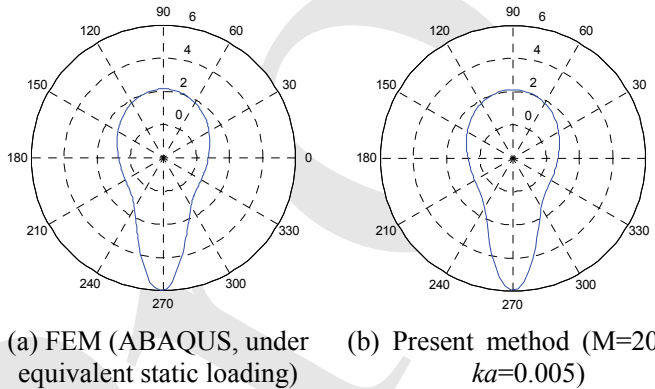


Figure 15: Distribution of DMCF on the upper circular boundary by using different methods, the present method and FEM ($L/a=2.1$)

326 Fourier coefficients of boundary densities have been determined, the flexural wave
 327 scattering field and dynamic moment concentrations can be obtained by using the
 328 boundary integral equations for domain points in conjunction with general rotated
 329 degenerate kernels. For an infinite plate with one hole, good agreement between
 330 the results of the present method and those of analytical solution is observed. For
 331 the cases of small wave number, the present results for a plate with one or multi-
 332 ple circular holes are well compared with the static case of finite element method

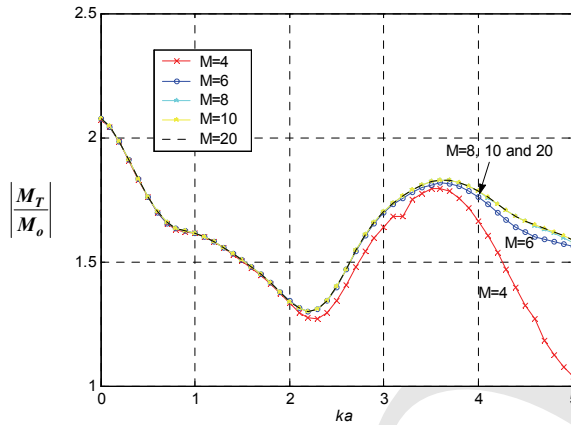


Figure 16: DMCF on the upper circular boundary ($\theta = -\pi/2$) versus the dimensionless wave number by using different number of terms of Fourier series ($L/a=4.0$)

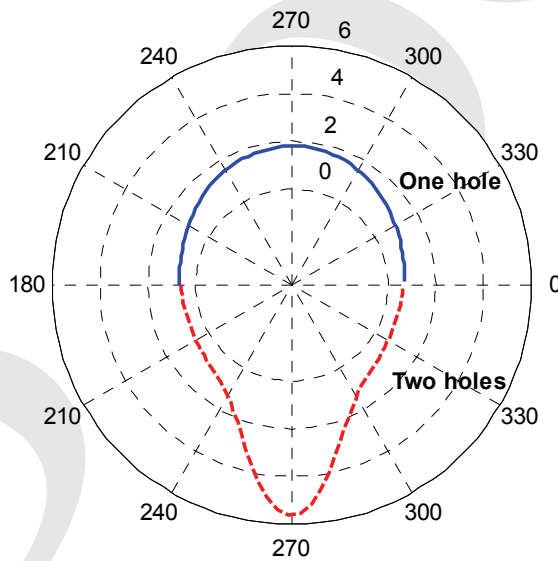


Figure 17: Distribution of DMCF $|M_T/M_0|$ on the circular boundary, solid line for one hole and dash line for the upper one of two holes ($L = 2.1a, ka = 0.2$)

333 (FEM) using ABAQUS. Convergence rate depends on two parameters of the inci-
 334 dent wave number and the central distance between two holes. Numerical results

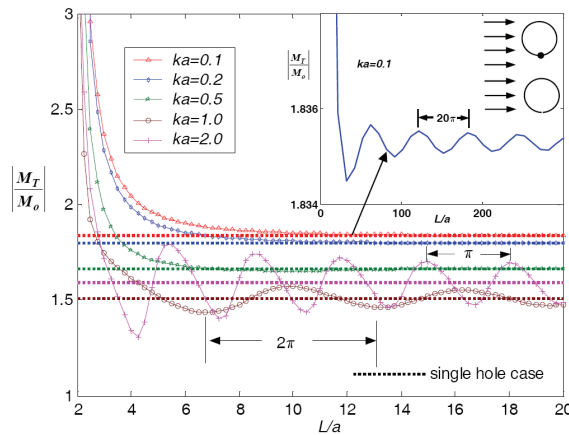


Figure 18: DMSF $|M_T/M_0|$ on the circular boundary ($\theta = -\pi/2$) versus the dimensionless central distance of two holes for different wave number under the incident wave with $\phi_0 = 0$

335 indicate that the DMCF of two holes is apparently larger than that of one hole when
 336 two holes are close to each other. Fictitious frequency of external problem can be
 337 suppressed by using the more number of Fourier series terms. The effect of the central
 338 distance on DMCF has been studied by using the present method and indicates
 339 a regular variation of DMCF as the central distance of two holes increasing. As can
 340 be seen from the numerical results, the present method provides a semi-analytical
 341 solution for dynamic moment concentration factors in infinite thin plates with multiple
 342 circular holes subject to the incident flexural wave, since its analytical solution
 343 is not yet available.

344 8 References

- 345 **Beskos, D. E.** (1997): Boundary element methods in dynamic analysis: part ζ^o
 346 (1986-1996). *Applied Mechanics Reviews ASME*, vol. 50, no.3, pp. 149-197.
- 347 **Chandrasekhar, B.; Rao, S. M.** (2007): Acoustic Scattering from Fluid Bodies
 348 of Arbitrary Shape. *CMES: Computer Modeling in Engineering and Sciences*, vol.
 349 21, No. 1, pp. 67-80.
- 350 **Chandrasekhar, B.** (2008): Node based Method of Moments Solution to Combined
 351 Layer Formulation of Acoustic Scattering. *CMES: Computer Modeling in*
 352 *Engineering and Sciences*, vol. 33, No. 3, pp. 243-267.
- 353 **Chen, H. B.; Fu, D. J.; Zhang, P. Q.** (2007): An Investigation of Wave Propa-

- 354 gation with High Wave Numbers via the Regularized LBIEM. *CMES: Computer*
 355 *Modeling in Engineering and Sciences*, vol. 20, No. 2, pp. 85-98.
- 356 **Chen, J. T.; Hong, H. K.** (1999): Review of dual boundary element methods
 357 with emphasis on hypersingular integrals and divergent series. *Applied Mechanics*
 358 *Reviews ASME*, vol. 52, no. 1, pp. 17-33.
- 359 **Chen, J. T.; Shen, W. C.; Chen, P. Y.** (2006a): Analysis of circular torsion bar
 360 with circular holes using null-field approach. *CMES: Computer Modeling in Engi-*
 361 *neering & Science*, vol. 12, pp. 109-119.
- 362 **Chen, J. T.; Hsiao, C. C.; Leu, S. Y.** (2006b): Null-field integral equation ap-
 363 proach for plate problems with circular holes. *Transactions of the ASME Journal*
 364 *of Applied Mechanics*, vol. 73, pp. 679-693.
- 365 **Chen, J. T.; Chen, C. T.; Chen, P. Y.; Chen, I. L.** (2007): A semi-analytical
 366 approach for radiation and scattering problems with circular boundaries. *Computer*
 367 *Methods in Applied Mechanics and Engineering*, vol. 196, pp. 2751-2764.
- 368 **Chen, J. T.; Ke, J. N.** (2008): Derivation of anti-plane dynamic green's function
 369 for several circular inclusions with imperfect interfaces. *CMES: Computer Model-*
 370 *ing in Engineering & Science*, vol. 29, pp. 111-135
- 371 **Gao, S. W.; Wang, B. L.; Ma, X. R.** (2001): Scattering of elastic wave and dy-
 372 namic stress concentrations in thin plate with a circular hole. *Engineering mechan-*
 373 *ics*, vol. 18, no. 2, pp. 14-20.
- 374 **Gao, S. W.; Wang, Y. S.; Zhang, Z. M.; Ma, X. R.** (2005): Dual reciprocity
 375 boundary element method for flexural waves in thin plate with cutout. *Applied*
 376 *Mathematics and Mechanics*, vol. 26, no. 12, pp. 1564-1573.
- 377 **Gradshteyn, I. S.; Ryzhik, I. M.** (1996): Table of integrals, series, and products.
 378 5th edition, Academic Press
- 379 **Hayir, A., Bakirtas, I.** (2004): A note on plate having a circular cavity excited by
 380 plane harmonic SH waves. *Journal of Sound and Vibration*, vol. 271, pp. 241-255.
- 381 **Hu, C.; Ma, X. R.; Huang, W. H.** (1998): Dynamic stress concentrations in thin
 382 plates with two circular cutouts. *Acta Mechanica Sinica*, vol. 30, no. 5, pp. 587-
 383 596.
- 384 **Hu, C.; Fang, X.; Huang, W.** (2007): Multiple scattering of flexural waves in a
 385 semi-infinite thin plate with a cutout. *International Journal of Solids and Struc-*
 386 *tures*, vol. 44, pp. 436-446.
- 387 **Hutchinson, J. R.** (1991): Analysis of plates and shells by boundary collocation.
 388 In: Beskos DE (ed) *Boundary Elements Analysis of Plates and Shells*. Springer
 389 Berlin, pp. 314-368.
- 390 **Kitahara, M.** (1985): Boundary integral equation methods in eigenvalue problems

- 391 of elastodynamics and thin plates. Elsevier, Amsterdam.
- 392 **Kobayashi, S.; Nishimura, N.** (1981): Transient Stress Analysis of Tunnels and
393 Caverns of Arbitrary Shape Due to Traveling Waves. in: *Developments in Bound-*
394 *ary Element Methods-II*, Banerjee, P. K., and Shaw, R. P., eds., Applied Science,
395 London, pp. 177-210.
- 396 **Kress, R.** (1989): Linear integral equations, Springer-Verlag, Berlin.
- 397 **Kung, George C. S.** (1964): Dynamical stress concentration in an elastic plate.
398 M.S. Thesis, Cornell University, Ithaca, NY.
- 399 **Leissa, W.** (1969): Vibration of plates. NASA SP-160.
- 400 **Lin, D.; Gai, B.; Tao, G.** (1982): Applications of the method of complex functions
401 to dynamic stress concentrations. *Wave Motion*, vol. 4, pp. 293-304.
- 402 **Martin, P. A.** (2006): Multiple scattering interaction of time-harmonic wave with
403 N obstacles. Cambridge University Press, UK.
- 404 **Nishimura, G.; Jimbo, Y.** (1955): A dynamical problem of stress concentration.
405 *Journal of the Faculty of Engineering*, University of Tokyo, Japan, vol. 24, pp.
406 101.
- 407 **Norris, A. N.; Vemula, C.** (1995): Scattering of flexural waves on thin plates.
408 *Journal of Sound and Vibration*, vol. 181, pp. 115-125.
- 409 **Pao, Y. H.; Mow, C. C.** (1972): Diffraction of elastic waves and dynamics stress
410 concentration. Crane, New York.
- 411 **Pao, Y. H.** (1962): Dynamical stress concentration in an elastic plate. *Transactions*
412 *of the ASME Journal of Applied Mechanics*, June, pp. 299-305.
- 413 **Squire, V. A.; Dixon, T. W.** (2000): Scattering of flexural waves from a coated
414 cylindrical anomaly in a thin plate. *Journal of Sound and Vibration*, vol. 236, no.
415 2, pp. 367-373.
- 416 **Tanaka, M.; Sladek, V.; Sladek, J.** (1994): Regularization techniques applied to
417 boundary element methods. *Applied Mechanics Reviews*, vol. 47, pp. 457-499.

418 **Appendix I: Degenerate kernels**

$$U^j(x, s) = \sum_{m=0}^{\infty} f_j \cos(m(\theta - \varphi_i)), \quad j = 1, 2$$

where

$$f_1 = \frac{1}{8k^2 D} \varepsilon_m \{ J_m(k\rho) [Y_m(kR) - iJ_m(kR)] + \frac{2}{\pi} I_m(k\rho) K_m(kR) \}$$

$$f_2 = \frac{1}{8k^2 D} \varepsilon_m \{ J_m(kR) [Y_m(k\rho) - iJ_m(k\rho)] + \frac{2}{\pi} I_m(kR) K_m(k\rho) \}$$

$$\Theta^j(x, s) = \frac{\partial U^j(x, s)}{\partial R} = \sum_{m=0}^{\infty} g_j \cos(m(\theta - \varphi)), \quad j = 1, 2$$

where

$$g_1 = \frac{1}{8kD} \varepsilon_m \{ J_m(k\rho) [Y'_m(kR) - iJ'_m(kR)] + \frac{2}{\pi} I_m(k\rho) K'_m(kR) \}$$

$$g_2 = \frac{1}{8kD} \varepsilon_m \{ J'_m(kR) [Y_m(k\rho) - iJ_m(k\rho)] + \frac{2}{\pi} I'_m(kR) K_m(k\rho) \}$$

where

$$\varepsilon_m = \begin{cases} 1 & m = 0 \\ 2 & m \neq 0 \end{cases},$$

the superscript j (1 or 2) denotes the interior domain (*i.e.* $\rho < R$, $j=1$) and exterior domain (*i.e.* $\rho > R$, $j=2$), respectively.

$$M^j(x, s) = \sum_{m=0}^{\infty} p_j \cos(m(\theta - \phi_i)), \quad j = 1, 2$$

where

$$p_1 = -\frac{1}{8k^2} \varepsilon_m \{ J_m(k\rho) [\alpha_m^Y(kR) - i\alpha_m^J(kR)] + \frac{2}{\pi} I_m(k\rho) \alpha_m^K(kR) \}$$

$$p_2 = -\frac{1}{8k^2} \varepsilon_m \{ \alpha_m^J(kR) [Y_m(k\rho) - iJ_m(k\rho)] + \frac{2}{\pi} \alpha_m^I(kR) K_m(k\rho) \}$$

$$\alpha_m^Y(kR) = k^2 Y_m''(kR) + \nu \left[\frac{k}{R} Y_m'(kR) - \frac{m^2}{R^2} Y_m(kR) \right]$$

$$\alpha_m^J(kR) = k^2 J_m''(kR) + \nu \left[\frac{k}{R} J_m'(kR) - \frac{m^2}{R^2} J_m(kR) \right]$$

$$\alpha_m^K(kR) = k^2 K_m''(kR) + \nu \left[\frac{k}{R} K_m'(kR) - \frac{m^2}{R^2} K_m(kR) \right]$$

$$\alpha_m^I(kR) = k^2 I_m''(kR) + \nu \left[\frac{k}{R} I_m'(kR) - \frac{m^2}{R^2} I_m(kR) \right]$$

$$V^j(x, s) = \sum_{m=0}^{\infty} q_j \cos(m(\theta - \phi_i)), \quad j = 1, 2$$

where

$$q_1 = -\frac{1}{8k^2}\varepsilon_m\{J_m(k\rho)[\beta_m^Y(kR) - i\beta_m^J(kR)] + \frac{2}{\pi}I_m(k\rho)\beta_m^K(kR)\}$$

$$q_2 = -\frac{1}{8k^2}\varepsilon_m\{\beta_m^J(kR)[Y_m(k\rho) - iJ_m(k\rho)] + \frac{2}{\pi}\beta_m^I(kR)K_m(k\rho)\}$$

$$\begin{aligned}\beta_m^Y(kR) &= k^3 Y_m'''(kR) + \frac{k^2}{R} Y_m''(kR) \\ &\quad - \frac{k}{R^2} [1 + (2 - \nu)m^2] Y_m'(kR) + \left[\frac{(3 - \nu)m^2}{R^3} \right] Y_m(kR)\end{aligned}$$

$$\begin{aligned}\beta_m^J(kR) &= k^3 J_m'''(kR) + \frac{k^2}{R} J_m''(kR) \\ &\quad - \frac{k}{R^2} [1 + (2 - \nu)m^2] J_m'(kR) + \left[\frac{(3 - \nu)m^2}{R^3} \right] J_m(kR)\end{aligned}$$

$$\begin{aligned}\beta_m^K(kR) &= k^3 K_m'''(kR) + \frac{k^2}{R} K_m''(kR) \\ &\quad - \frac{k}{R^2} [1 + (2 - \nu)m^2] K_m'(kR) + \left[\frac{(3 - \nu)m^2}{R^3} \right] K_m(kR)\end{aligned}$$

$$\begin{aligned}\beta_m^I(kR) &= k^3 I_m'''(kR) + \frac{k^2}{R} I_m''(kR) \\ &\quad - \frac{k}{R^2} [1 + (2 - \nu)m^2] I_m'(kR) + \left[\frac{(3 - \nu)m^2}{R^3} \right] I_m(kR)\end{aligned}$$

where

$$\varepsilon_m = \begin{cases} 1 & m = 0 \\ 2 & m \neq 0 \end{cases},$$

419 the superscript j (1 or 2) denotes the interior domain (*i.e.* $\rho < R$, $j=1$) and exterior
420 domain (*i.e.* $\rho > R$, $j=2$), respectively.

421 **Appendix II: Degenerate kernels with respect to the adaptive observer system**

The expressions for U_θ , Θ_θ , M_θ and V_θ can be obtained by replacing L in Eq.(A1) by U , Θ , M and V , and replacing h in Eq.(A1) by f, g, p and q , respectively. The definition of U , Θ , M , V , f, g, p and q can be seen in the Appendix I.

$$L_\theta^j(x, s) = \sum_{m=0}^{\infty} c_1 h'_j \cos(m(\theta - \varphi_i)) + s_0 h_j \sin(m(\theta - \varphi_i)), \quad j = 1, 2 \quad (A1)$$

where $c_1 = \cos(\delta_i)$, $s_0 = \left(\frac{m}{\rho_i}\right) \sin(\delta_i)$ and $\delta_i = \phi_c - \phi_i$. The expressions for U_m , Θ_m , M_m and V_m can be obtained by replacing L in Eq.(A2) by U , Θ , M and V , and replacing h in Eq.(A2) by f, g, p and q , respectively

$$L_m^j(x, s) = \sum_{m=0}^{\infty} [mc_0 h_j + mc_1 h'_j + mc_2 h''_j] \cos(m(\theta - \varphi_i)) + [ms_0 h_j + ms_1 h'_j] \sin(m(\theta - \varphi_i)), \quad j = 1, 2 \quad (A2)$$

where

$$mc_0 = -\left(\frac{m^2}{2\rho_i^2}\right) (1 + \nu + (-1 + \nu)\cos(2\delta_i)),$$

$$mc_1 = \left(\frac{1}{2\rho_i}\right) (1 + \nu + (-1 + \nu)\cos(2\delta_i)),$$

$$mc_2 = \left(\frac{1}{2}\right) (1 + \nu + (1 - \nu)\cos(2\delta_i)),$$

$$ms_0 = \left(\frac{m}{\rho_i^2}\right) (-1 + \nu)\sin(2\delta_i),$$

$$ms_1 = \left(\frac{m}{\rho_i}\right) (1 - \nu)\sin(2\delta_i),$$

422 the superscript j (1 or 2) denotes the interior domain (*i.e.* $\rho < R$, $j=1$) and exterior
 423 domain (*i.e.* $\rho > R$, $j=2$), respectively.